SPE-173227-MS

An Efficient Adaptive Nonlinearity Elimination Preconditioned Inexact Newton Method for Parallel Simulation of Thermal-Hydraulic-Mechanical Processes in Fractured Reservoirs

Shihao Wang, Philip H. Winterfeld, and Yu-Shu Wu, Colorado School of Mines

This paper was prepared for presentation at the SPE Reservoir Simulation Symposium held in Houston, Texas, USA, 23–25 February 2015.

Abstract

In this paper, we introduce a physics-based nonlinear preconditioner, based on the Inexact Newton method, to accelerate the highly nonlinear thermal-hydraulic-mechanical (THM) simulation of fractured reservoirs. Inexact Newton method has become a popular iterative solver for solution of partial differential equations (PDE). Instead of solving the PDEs exactly with the expensive Newton method, the Inexact Newton method finds a direction for the iteration and solves the equations inexactly. The Inexact Newton method is very efficient when the initial guess is close to the objective solution. However, when the equations are not smooth enough, especially when local discontinuities exits, the Inexact Newton method may be slow or even stagnant.

Local discontinuities are commonly encountered during oil and gas flow in reservoirs. One problem that involves lots of local discontinuities is the simulation of multiphase flow in fractured reservoirs. Fractures in petroleum reservoirs are typically sensitive to the change of pressure and stress. The thermal-hydraulic-mechanical (THM) effects of injection and production can dramatically change the properties of fractures, resulting in a huge variation in the permeability, which adds nonlinearity to the governing partial differential equations. Considering these characteristics of fractured reservoirs, applying the Inexact Newton method directly to them faces severe difficulties. In this work, we have proposed and studied a nonlinear preconditioner to resolve the above problem. In this nonlinear preconditioner, a restricted additive Schwarz approach is used to coarsen the problem and the Inexact Newton method is used as a global iterative solver. We have developed a physics-based strategy to adaptively identify the highly nonlinear zones by computing and comparing the gradient of the stress/temperature-permeability correlations of the fractured zones. These nonlinear zones are treated as a subspace problem, which is solved locally. The results of the subspace problem are used to modify the global residual. By conducting the above operations, the local nonlinearity is eliminated and the global iteration is accelerated. An adaptive strategy is adopted to dynamically choose between the Inexact Newton method and the Newton method.

The above algorithm has the advantage of remarkable scalability and is easy to implement in massively parallel reservoir simulators. We have programed the algorithm and implemented it into our fully coupled,

fully implicit THM reservoir simulator to study the effects of cold water injection on fractured reservoirs. The numerical and parallel framework of the simulator has been described by Wang et al. (2014). Previously, the cold water injection problem suffered from slow convergence at the injection zone where fracture permeability changes rapidly. The results of this work show that after the implementation of this nonlinear preconditioner, the iterative solver has become significantly more robust and efficient.

Introduction

The Inexact Newton method with Backtracking (INB) solves a nonlinear system approximately within each iteration. It can save much computational time spent that would otherwise be used for the linear solver. However, one of the drawbacks of the INB algorithm is that it is not as robust as Newton-Raphson algorithm (NR) in certain cases. For INB algorithm, it has been proven by Cai and Li. (2011) that if the target nonlinear equation is continuously differentiable and there is a limit point at which the Jacobian matrix is nonsingular, then the INB converges at that limit point. With the existence of local discontinuities, the target equation is no longer continuously differentiable and the more the discontinuities, the farther the system is away from a continuously differential condition. Therefore as the number of local discontinuities increases, INB may suffer from convergence problems.

For several types of reservoir simulation problems, such as water-oil displacement, nonlinearity exists only in a small portion of the entire field. This local nonlinearity will dramatically slow down the convergence of nonlinear solvers. For the INB method, if the local nonlinearity is too high, the iteration will tend to be stagnant. Therefore, to guarantee the robustness of the INB, a nonlinear preconditioner is typically required, such as the Addictive Schwarz Preconditioned Inexact Newton (ASPIN), as proposed by Cai and Keyes. (2002). Recently, ASPIN has been applied to groundwater and oil simulation problems by Skogestad et al. (2013) and Sun et al. (2013), respectively. ASPIN has been shown to be able to improve the convergence rate for highly heterogeneous reservoir simulation problems. However, as far as we know, there have no attempts to adopt the nonlinearity elimination (NE) technique to precondition reservoir simulation problems that have high nonlinearity on certain areas of the computational domain.

In this work, we propose another type of preconditioned INB method to deal with the local nonlinearity problems. We aim to eliminate the local discontinuity to enhance the numerical performance of the INB algorithm. Nonlinearity elimination techniques for INB have been studied by Hwang et al. (2010, 2014) with Computational Fluid Dynamics (CFD) problems. In this work, we will introduce an adaptive nonlinearity elimination (ANE) algorithm. This ANE algorithm adopts a physics based criterion to choose a highly nonlinear region out of the computational domain and eliminates the local nonlinearity before the start of INB. The highly nonlinear region can be adaptively chosen in each time step. Hwang et al. (2014) first proposed such combined ANE-INB approach and applied it to the solution of the transonic full potential equation. In their work, the target equation is in steady state. In this work, we will implement ANE-INB into a transient reservoir simulation problem. We will investigate the performance of ANE-INB in the study of coupled THM behavior of fractured reservoirs, especially for the elastic-plastic responses of fractures induced by cold water injection into oil/gas reservoirs. Moreover, as our simulator is massively parallel, we implement a restricted Schwarz nonlinear preconditioner to balance the nonlinearity. The restricted Schwarz preconditioner can be conveniently implemented in an existing code with very little additional communication and computation.

Problem Description

Governing Equations

We have developed a massively parallel simulator to study the coupled thermal-hydraulic-mechanical (THM) behavior of fractured reservoirs. The simulator is based on the framework of MSFLOW (Wu. 1998) and is able to simultaneously solve the coupled thermal-hydraulic-mechanical field of fractured reservoirs. The governing equation for hydraulic and thermal flow is as follows

$$\frac{dM^k}{dt} = \nabla \cdot \vec{F}^k + q^k \tag{1}$$

In our simulator, k=1 refers to the hydrocarbon component; k=2 refers to the water component; k=3 refers to heat. In the above equation, q is the sink/source term; M is the conserved component in-place; and F is the flux. For water/oil equations, the mass componenent in-place is,

$$M^k = \phi \sum_\beta S_\beta \rho_\beta \tag{2}$$

where ϕ is the rock porosity; S_β and ρ_β are the saturation and density of phase β, respectively.

The flux term is given by,

$$\vec{F}_\beta^{k=1,2} = -K \frac{K_{r\beta}\rho_\beta}{\mu_\beta}\left(\nabla P_\beta - \rho_\beta \boldsymbol{g}\right) \tag{3}$$

where K is the absolute permeability; P_β is the pressure of phase β; $K_{r\beta}$ and μ_β are the relative permeability and viscosity of phase β, respectively; and g is the gravitational acceleration vector.

The heat flux term includes conduction and convection,

$$\vec{F}^{k=3} = -\left[\left(1-\phi\right)K_R + \phi \sum_\beta S_\beta K_\beta\right]\nabla T + \sum_\beta h_\beta \vec{F}_\beta \tag{4}$$

where and K_R and K_β are thermal conductivity of the rock and the liquid phase, β, respectively; $\vec{F}_\beta$ is the liquid flux term used in the oil/water equation; T is temperature; and h_β is enthalpy of liquid phase β. The accumulation term for the heat equation is the following,

$$M^\kappa = (1-\phi)\rho_R C_R T + \phi \sum_\beta S_\beta \rho_\beta u_\beta \tag{5}$$

where ρ_R and C_R are the density and heat capacity of rock, respectively; and u_β is the internal energy of liquid phase β.

For the mechanical simulation, we start from the following displacement equation for a thermo-poroelastic material (Winterfeld and Wu, 2014),

$$\alpha \nabla P + 3\beta K \nabla T + \left(\lambda + G\right)\nabla\left(\nabla \cdot \vec{u}\right) + G\nabla^2 \vec{u} + \vec{F} = 0 \tag{6}$$

where α is the Biot's coefficient; λ is the Lame's parameter; G is the shear modulus; and $\vec{F}$ is the body force and $\vec{u}$ is the displacement vector.

The normal stresses appearing in Hooke's law for a linear thermo-poro-elastic material are,

$$\sigma_{kk} - \left(\alpha P + 3\beta K\left(T - T_{ref}\right)\right) = \lambda \varepsilon_v + 2G\varepsilon_{kk}, k = x, y, z \tag{7}$$

where σ_{kk} is the normal stress along the kth direction; β is the thermal expansion coefficient; T_{ref} is a reference temperature; and ε_v is the volumetric strain; and the summation of normal strain ε_{kk} is over the three directions,

$$\varepsilon_v = \varepsilon_{xx} + \varepsilon_{yy} + \varepsilon_{zz} \tag{8}$$

We introduce the mean stress σ_m as follows,

$$\sigma_m = \frac{\sigma_{xx} + \sigma_{yy} + \sigma_{zz}}{3} \tag{9}$$

Then, after several steps of derivation, we arrive at the governing mean stress equation (Winterfeld and Wu, 2014),

$$\frac{3(1-\nu)}{(1+\nu)}\nabla^2\sigma_m+\nabla\cdot\vec{F}=\frac{2(1-2\nu)}{(1+\nu)}\left(\alpha\nabla^2P+3\beta K\nabla^2T\right) \tag{10}$$

Integral Finite Difference (IFD) Method

We use Integral Finite Difference (IFD) method to solve the above governing equations. By integrating each conservation equation over a representative element volume (REV), we get the following integrated governing equation,

$$\frac{d}{dt}\int_{V_n}M^k dV_n=\int_{\Gamma_n}\vec{F}^k\cdot\vec{n}d\Gamma_n+\int_{V_n}q^k dV_n \tag{11}$$

Using the IFD method, the governing equations are discretized as the following general form,

$$\frac{\left(V^{i+1}M^{k,i+1}-V^iM^{k,i}\right)}{\Delta t}=\sum_m A_{nm}F^k_{nm}+q^k \tag{12}$$

The details of the simulator framework and this IFD implementation can be found in (Winterfeld and Wu, 2014). The above equation is solved by our proposed nonlinear solvers, to be described in the next session.

Cold Water Injection Induced Fracture Aperture Change

For fractured reservoirs, the fractures are sensitive to coupled THM effects. In this work, we first propose a semi-analytical correlation of the fracture aperture change induced by cold water injection. Consider the dual continua matrix-fracture system. We focus on a matrix block surrounded by fractures of length L_i on the ith direction. The temperature and pressure in the fractures are kept constant as P_f and T_f, respectively. The initial temperature and pressure of the matrix block are P_{m0} and T_{m0}, respectively. For a 1-D problem, and ignoring leak-off into the matrix block, the temperature distribution inside the matrix rock can be solved analytically from the governing heat equation as,

$$T_m=T_f+\sum_{n=1}^{\infty}\frac{4\left(T_{ini}-T_f\right)}{(2n-1)\pi}\sin\left[\frac{(2n-1)\pi}{L_i}x\right]e^{-\frac{K_R}{\rho_R C_R}\frac{(2n-1)^2\pi^2}{L_i^2}t} \tag{13}$$

where T_{ini} is the initial temperature of the system and L_i is the fracture spacing.

We obtain the displacement distribution inside the matrix block using an analytical solution. We rewrite the displacement equation in three dimensions as follows,

$$\alpha\frac{\partial P}{\partial x}+3\beta K\frac{\partial T}{\partial x}+(G+\lambda)\left(\frac{\partial^2u_x}{\partial x^2}+\frac{\partial^2u_y}{\partial x\partial y}+\frac{\partial^2u_z}{\partial x\partial z}\right)+G\left(\frac{\partial^2u_x}{\partial x^2}+\frac{\partial^2u_x}{\partial y^2}+\frac{\partial^2u_x}{\partial z^2}\right)+F_x=0 \tag{14}$$

$$\alpha\frac{\partial P}{\partial y}+3\beta K\frac{\partial T}{\partial y}+(G+\lambda)\left(\frac{\partial^2u_x}{\partial x\partial y}+\frac{\partial^2u_y}{\partial y^2}+\frac{\partial^2u_z}{\partial y\partial z}\right)+G\left(\frac{\partial^2u_y}{\partial x^2}+\frac{\partial^2u_y}{\partial y^2}+\frac{\partial^2u_y}{\partial z^2}\right)+F_y=0 \tag{15}$$

$$\alpha\frac{\partial P}{\partial z}+3\beta K\frac{\partial T}{\partial z}+(G+\lambda)\left(\frac{\partial^2u_x}{\partial x\partial z}+\frac{\partial^2u_y}{\partial y\partial z}+\frac{\partial^2u_z}{\partial z^2}\right)+G\left(\frac{\partial^2u_z}{\partial x^2}+\frac{\partial^2u_z}{\partial y^2}+\frac{\partial^2u_z}{\partial z^2}\right)+F_z=0 \tag{16}$$

If we ignore leak-off and rewrite the 1-D version of the governing displacement equation with respect to matrix block as,

$$3\beta K\frac{\partial T}{\partial x}+(2G+\lambda)\frac{\partial^2u_x}{\partial x^2}=0 \tag{17}$$

and implement the following boundary conditions,

$$\Delta\sigma_{xx}=-k_fu_x-\Delta P_f \quad \text{at } x=L_i/2 \tag{18}$$

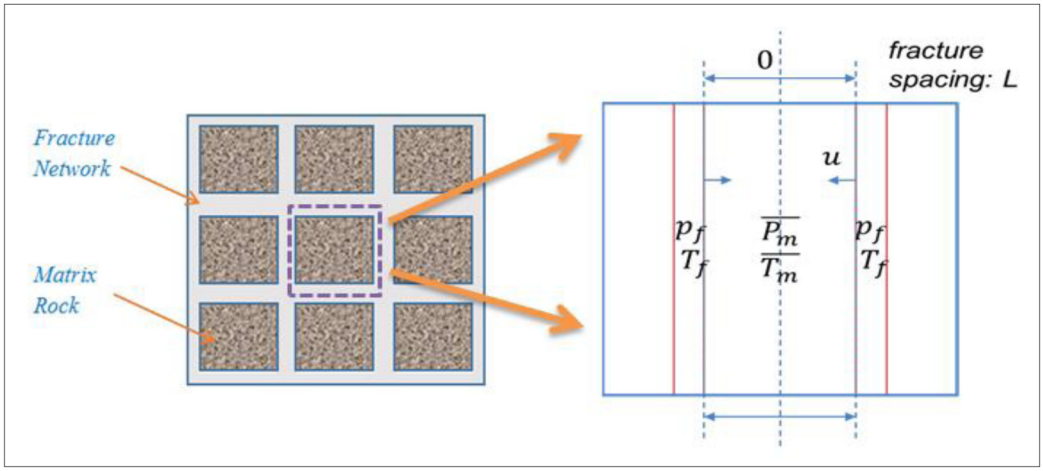

Figure 1—Conceptual model of fracture-matrix network

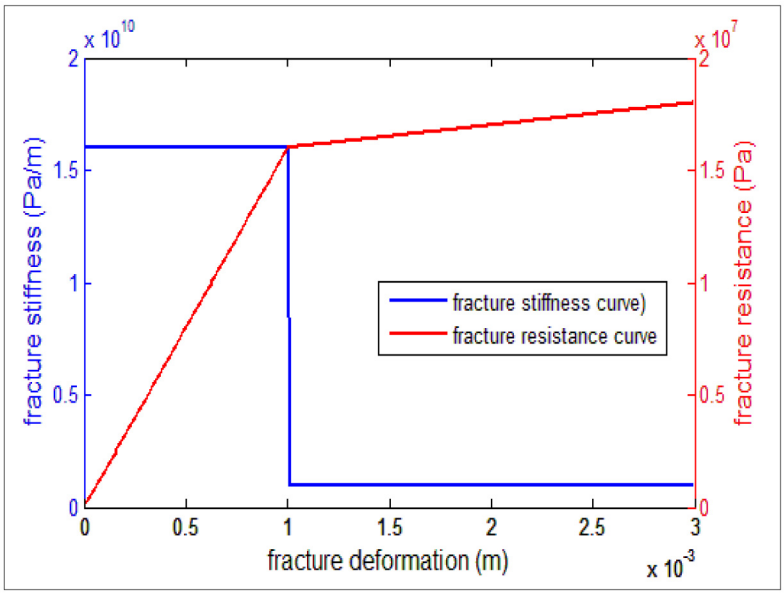

Figure 2—Elastic-plastic deformation of fracture. Blue line: fracture stiffness curve. Red line: fracture resistance curve.

$$u_x = 0 \quad \text{at } x = 0 \tag{19}$$

where k_f is the 'stiffness' the fracture and $k_f u_x$ is the resistance of the fracture. The displacement at the fracture-matrix interface is then solved as,

$$u_i\left(\frac{L_i}{2}\right) = \frac{-(P_f - P_{f,0}) + \beta(\overline{T_m} - T_{m,0})\frac{E_m}{1-2\nu}}{\frac{E_m}{1-2\nu} + k_f L_i/2} \cdot \frac{L_i}{2} \tag{20}$$

The fracture aperture change Δb_i is,

$$\Delta b_i = -2\Delta u_i\left(\frac{L_i}{2}\right) \tag{21}$$

Therefore, the fracture aperture change can be expressed as

$$\Delta b_i = \frac{(P_f - P_{f,0}) - \beta(T_m - T_{m,0})\frac{E_m}{1-2\nu}}{\frac{E_m}{1-2\nu} + k_f L_i/2} \cdot L_i \tag{22}$$

Fracture permeability can be calculated using the cubic law as,

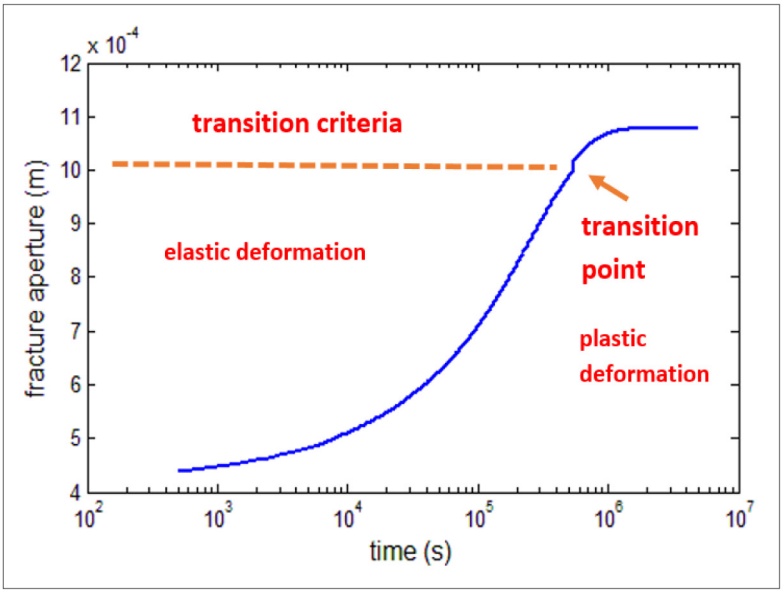

Figure 3—Elastic-plastic fracture aperture change. The arrow indicate the transition point from elastic deformation region to plastic deformation region.

$$K_{fi} = C_i \frac{(b_{i0}+\Delta b_i)^3}{12L_i} \tag{23}$$

where C_i is a parameter to correlate between the mechanical aperture and the hydraulic aperture. In this work, C_i is set to be 1.

The correlation can be also applied to cases where the fractures have elastic-plastic resistance. If the fracture is treated as elastic-plastic material, then the fracture has different stiffness within elastic and plastic zone. When deformantion is relatively small, the fracture has elastic behaviors with constant elastic stiffness. The fracture resistance transit into plastic material, when the entire the fracture aperture change exceed a certain 'breaking' criteria. For example, we assume the deformation at which fracture breaks is 1 mm ($3.2*10^{-3}$ ft). Within the elastic zone, the resistance of the fracture is set to be 16 GPa/m (250000 psi/ft.). Within the plastic zone, the resistance of the fracture is set to be 1 GPa/m (16000 psi/ft), as shown in Fig 2.

With the above fracture properties, for a typical reservoir with a fracture spacing of 20 inches (0.508 m), the fracture aperture change curve of each grid block is similar to the curve shown in the following figure,

As demonstrated by the above figures, the fracture stiffness has a 'plunge' at the transition point. Once the elastic-plastic transition point is reached, the fracture stiffness suddenly drops, resulting in a discontinuity of the fracture permeability. The fracture aperture rapidly increases by 200% to 300% and exceeds the elastic region. Because of the cubic law, the fracture permeability will increase accordingly by one order of magnitude. The above change of fracture permeability takes place within the time period of less than one day, which is smaller than the usually time step in reservoir simulation. Actually we have observed frequent time step cut during the simulation run using either Newton method or Inexact Newton method.

Description of algorithm

As described in the above section, a local discontinuity exists in the cold water injection problem. In this section, we describe the nonlinearity elimination Inexact Newton method. Suppose the THM coupled nonlinear system is,

$$F(x)=0 \tag{24}$$

We consider the nonlinear equations resulting from integral finite difference method as,

$$\boldsymbol{J}(x)\boldsymbol{X}=\boldsymbol{R} \tag{25}$$

where $J(x)$ is the Jacobian matrix; X is the primary variable array; and R is the residual vector.

Restriction of Highly Nonlinear Region

Within each time step, before the start of the Inexact Newton iteration, we first eliminate the local nonlinearity to smooth the nonlinear equations. We firstly divide the entire set of all grid blocks, S, into two sets: grid blocks with high nonlinearity S^h and grid blocks with low nonlinearity S^l.

$$S=S^h \bigcup S^l \tag{26}$$

S^h contains all grid blocks, whose nonlinearity has not been eliminated yet. Then we define two restrictors, R_h and R_l, which restrict the entire system to the high nonlinearity and low nonlinearity subdomains, respectively,

$$F_{S_h}(x)=R_h F(x) \tag{27}$$

$$F_{S_l}(x)=R_l F(x) \tag{28}$$

Then we solve the subspace problem

$$F_{S_n^k}(R_l x^k + C_h) = 0 \; for \; C_h \tag{29}$$

where C_h^k is the subspace correction. Then we update the primary variables as$x = R_l^n x + C_h$

This way, the local nonlinearity is eliminated by the above restriction before the start of nonlinear iterations. This local nonlinearity elimination step can be view as a preliminary nonlinear preconditioner. As observed by Hwang et al. (2014), this preliminary elimination process only requires one or two iterations. This step eliminates the local nonlinearity within a very small region of the whole domain. The region can be adaptively chosen using a physics-based criteria. Since the number of highly nonlinear grid blocks is typically much smaller compared to the total number of grid blocks, the subspace problem can be simulated by one or two processors and without an elaborate domain partitioning. With the preliminary preconditioner, the nonlinearity can be eliminated more efficiently, as shown below.

Inexact Newton with Backtracking

After the preliminary nonlinearity elimination, we solve the resulting nonlinear system using restricted Schwarz preconditioned Inexact Newton with Backtracking method. We first describe the INB. Within the k^{th} iteration, INB solves the system $J(x^k)\, S^k = -Rx^k$ approximately and update x^k as,

$$x^k = x^k + \lambda^k s^k \tag{30}$$

until

$$\left\| R\left(x^k\right) + \lambda^k J^{-1}\left(x^k\right) R\left(x^k\right) \right\| \le \eta \left\| R\left(x^k\right) \right\| \tag{31}$$

where λ^k is the damping (linesearch) parameter ranging from 0 to 1. It shortens the Newton steps to enhance the robustness of the iteration. η is the forcing term. If η is 0, INB reduces to Newton method. In this work, η is set to be constant as 10^{-4}.

Restricted Schwarz Preconditioning

The restricted Schwarz preconditioning step is called between two INB steps. We partition the grid domain into N non-overlapping subdomains S_i^0 ,

$$\bigcup_{i=1}^{N} S_i^0 = S \tag{32}$$

Such partition can be assisted by existing packages, such as METIS (Karypis and Kumar, 1995). Then, we define the 1-level overlapping subdomain S_i^1 . For S_i^1 , every two subdomain overlaps with each other for 1-level, which means there is a 'rim' for each subdomain locating in its neighboring subdomains.

After defining the subdomains, we can define restrictors R_i^0 and R_i^1 which restricts the nonlinear system on S to subdomain S_i^0 and S_i^1 , respectively. A restrictor drops off the component outside its according subdomain and only keeps those components belonging to the according subdomain. Note here unlike S^h and S^q, these N subdomains will not adaptively change during the simulation.

$$F_i^1(x) = R_i^1 F(x) \tag{33}$$

Each subdomain solves the local problems approximately in parallel using INB method,

$$F_i^1\left(x^k + v_i^1\right) = 0 \tag{34}$$

where v_i^1 is the correction for subdomain i. The boundary condition for each subdomain uses the primary variables in the last time step of its neighboring subdomain. Here the information on the overlapping part of each pairs of subdomains is dropped. Such treatment is called the restricted Schwarz method. It has been observed by Cai and Li (2011) that the restricted Schwarz method has faster convergence rate and less communication,

$$x^k = \sum_{i=1}^{N} R_i^0\left(x^k + v_i^1\right) \tag{35}$$

The restricted Schwarz step aims to balance the nonlinearity among different processors; in this step, the stopping criteria is set as follows. For each type of equation, $j(j = 1,2,3,4)$ evaluate the norm of the residual $\left\|R_{1,j}^1\left(x^k\right)\right\| \ldots \left\|R_{N,j}^1\left(x^k\right)\right\|$. Let $\left\|R_{m,j}^1\left(x^k\right)\right\| = \max\left\{\left\|R_{i,j}^1\left(x^k\right)\right\| \mid 1 \le i \le N\right\}$, therefore $\left\|R_{m,j}^1\left(x^k\right)\right\|$ is the largest residual of the jth type of equation among all the subdomains. The nonlinearity is balanced only when,

$$\left\|R_{m,j}^1\left(x^k\right)\right\| < \rho_j \left\|R\left(u^k\right)\right\| \quad for \quad j = 1,2,3,4 \tag{36}$$

where the parameter ρ_j is a tolerance, chosen by the user. In this work, ρ_j is set as 0.75, as suggested by Cai and Li (2011).

This nonlinearity balance step can be viewed as a preconditioner that is implemented between two INB steps.

To briefly sum up, our approach implements a nonlinearity elimination preconditioner firstly to preliminarily reduce the local discontinuity. Then a restricted Schwarz preconditioner is called between INB steps to balance the nonlinearity among all processors. By conducting these operations, we aim to eliminate the effect of local discontinuity from global iterations in order to improve the robustness of INB. A flowchart of this proposed algorithm showing all operations in sequence is as follows.

Numerical Results

Problem Setup

We consider the type of cases in which one cold water injector and one production well locate symmetrically at the two boundaries of a fractured reservoir. The size of the reservoir is 760.00 m*760.00 m*50.00 m. The reservoir is divided into 80*80*15=96000 structured grid blocks. The initial pressure is 5.00 MPa and the initial temperature is 368 K (203 °F). Cold water is injected for 5 years at a constant rate of 1.0 kg/s (~ 545 bbl/d) from the injection well. The production well is producing at a constant bottom hole pressure of 3.0 MPa. The reservoir is 3 km in depth. The vertical in-situ stress is estimate from the density of caprock, which is assumed to be sandstone. Therefore the vertical in-situ stress v_z is

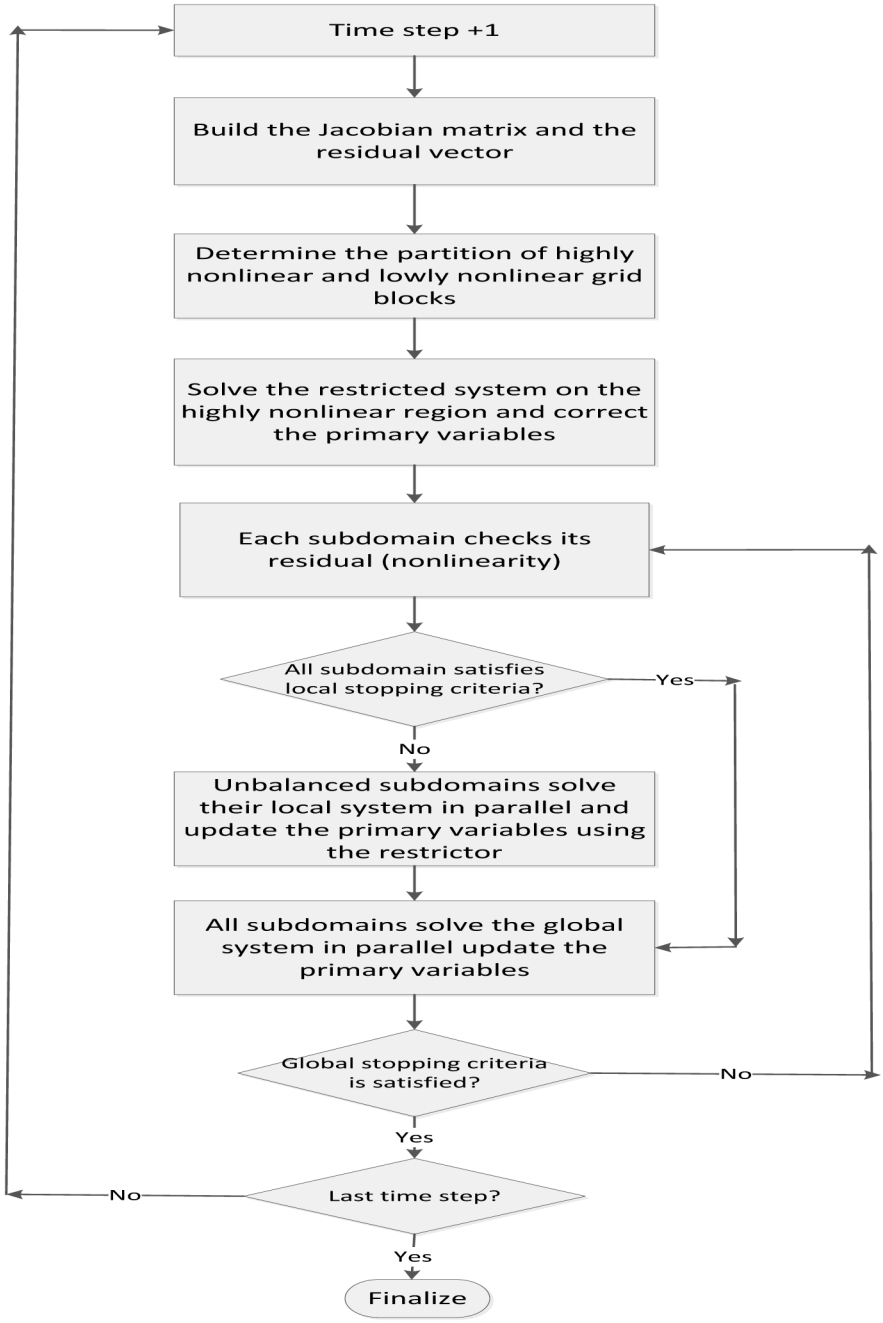

Figure 4—Flowchart of INB-ANE, showing the sequence of all operations within one time step.

73.50 MPa. The minimum horizontal stress $v_{min,hor}$ and maximum horizontal stress $v_{max,hor}$ are both set to be 51.45 MPa, which is 70% of the vertical in-situ stress. The rock properties are listed in Table 1. We will investigate the numerical performance of INB-ANE with different combinations of injection temperature, initial fracture permeability and breaking criteria. 8 cases have been run, the input parameters of which are shown in Table 2. Each case is run by 8 processes in parallel. Note here we treat the fracture permeability as a isotropy diagonal vector.

Chosen of Nonlinearity Elimination Criteria

The nonlinearity elimination criteria determines the high nonlinearity zone. In this problem, the nonlinearity is mainly the local discontinuity introduced by the failure of fractured material. We set the

Table 1—List of input properties of the rock

Properties	Values	Units
Initial permeability of the matrix	$K_{mx} = K_{mx}$=1.0*10-15 K_{mz} =1.0*10-15	m2
Initial porosity of the matrix	0.15	dimensionless
Initial porosity of the fracture	0.001	dimensionless
Young's modulus	16.0	GPa
Fracture spacing	0.5	m
Poisson's ratio	0.25	dimensionless
Biot's coefficient	1.0	dimensionless
Linear thermal expansion coefficient	11.6	10-6 m/(m K)
Thermal conductivity of dry rock	1.0	W/(m K)
Heat capacity of rock	1,000	J/(kg K)
Density of rock	2.5	103 kg/m3
v_z	73.50	MPa
$v_{min,hor}$	51.45	MPa
$v_{max,hor}$	51.45	MPa
Elastic resistance	12.0	GPa
Plastic resistance	0.7	GPa

Table 2—Input parameters for Case 1 to 8.

Case index	Injection Temperature (K)	Initial fracture permeability (m^2)	Breaking criteria (transition aperture) ($*10^{-6}$ m)
1	288.00	$1.00*10^{-11}$	200.00
2	288.00	$1.00*10^{-11}$	250.00
3	288.00	$5.00*10^{-12}$	200.00
4	288.00	$5.00*10^{-12}$	250.00
5	298.00	$1.00*10^{-11}$	200.00
6	298.00	$1.00*10^{-11}$	250.00
7	298.00	$5.00*10^{-12}$	200.00
8	298.00	$5.00*10^{-12}$	250.00

nonlinearity elimination criteria based on the relationship between the deformation (aperture change) Δb and the critical (breaking) deformation Δb_c of the fractured material as follows. For a given grid block v, suppose

$$\Delta b(v) = \theta \Delta b_c \tag{37}$$

where θ is a dynamically changing value.

The judgment that whether v belongs to the high nonlinearity region is made as

$$if \quad \theta(v)\epsilon(0.4, 1,2) \qquad v \in S^h; \tag{38}$$

$$else \qquad v \in S^l. \tag{39}$$

We adopt Case 1 as an example. For this case, the injection temperature is 288 K and the breaking deformation Δb_c is 200 μm. The initial fracture aperture can be calculated as 350 μm. Then according to Equ. 38 and 39, a grid block belongs to the high nonliearity group if its aperture change is between 430 μm to 590 μm. For the grid block locating at the injection point in Case 1, its fracture aperture change curve is shown in Fig 6. According to Fig 6, the grid block belongs to the high nonlinearity region between 1.0E6s (11.5 day) to 7.3E6s (84.5 day). We plot the permeability field at 180 days and 7 years after the start of the injection in Fig 7. Also, we plot the according distribution of the high/low nonliearity regions in Fig 8. By comparing Fig 7 and Fig 8, we can see that as the permeability enhancement effect propates,

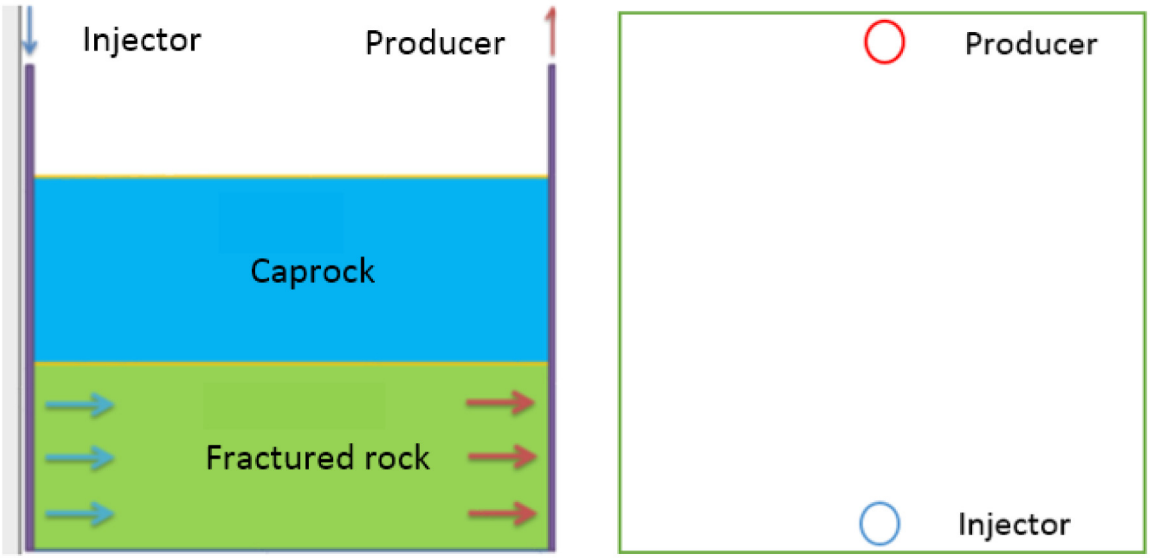

Figure 5—Problem setup. Left: side view of the reservoir, showing the fractured rock system and the fluid flow direction. Right: vertical view of the reservoir, showing the positions of the injector and the producer.

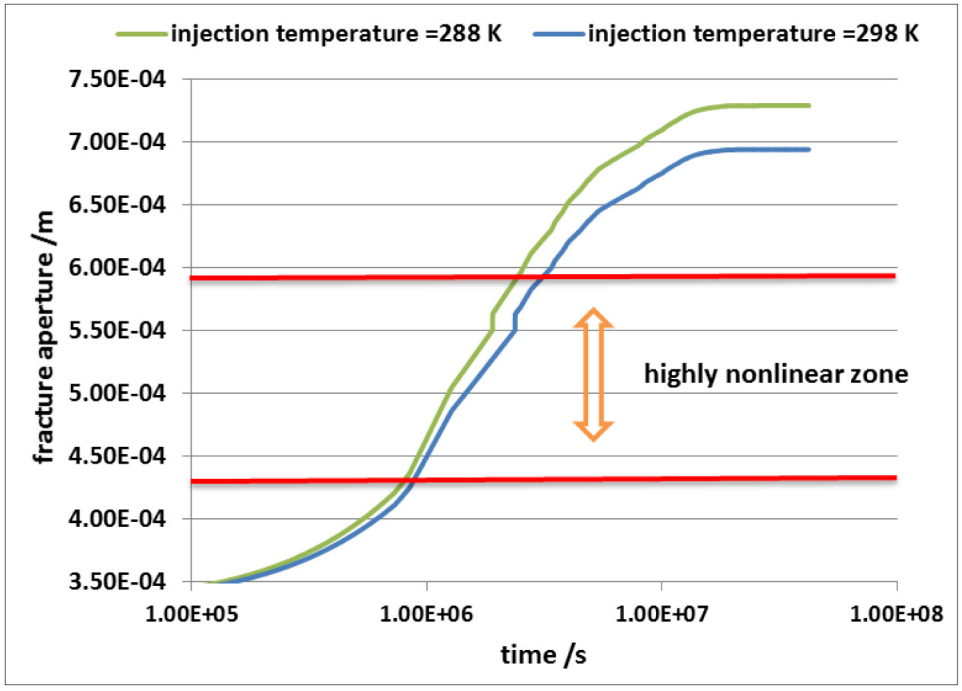

Figure 6—Fracture aperture curve at the cold water injector of Case 1 and Case 5. Red lines indicating the highly nonlinear zone determined by the judging criteria.

the highly nonlinearity region is around the heat front region. Besides, in either time point, the highly nonlinearity region is a small portion of the entere domain.

Numerical Performance

The average number of iterations per time step and the average on-wall computing time per time step are shown in Fig. 9 to Fig. 12. As the results demonstrates, the average number of iterations per time step of INB-ANE is in the range to 4 to 6, comparable to that of NR method and much less than of INB without preconditioning. It turns out that by implementing such a preconditioner, INB becomes more efficient and

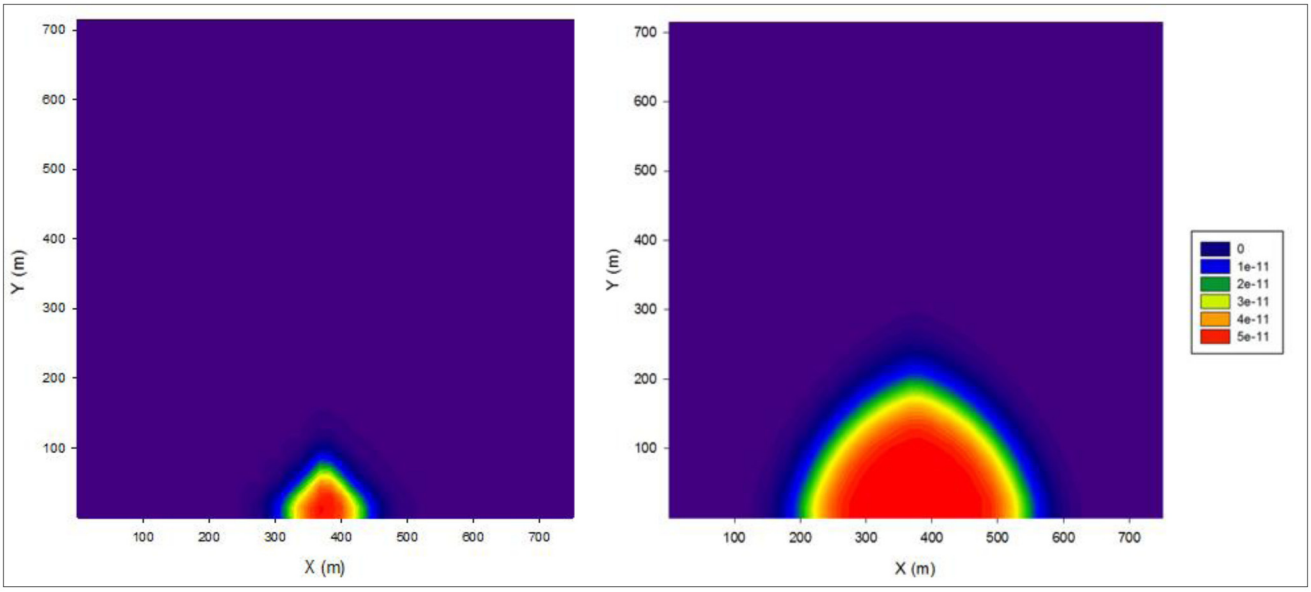

Figure 7—Permeability field of Case 1 after cold water injection. The unit of the fracture permeability is m^2. Red/orange color indicates the permeability enhanced zone near the injector. The figure on the left is the y-permeability field at 180 days of injection, while the figure on the right is the y-permeability field at 7 years of injection. In this case, the initial fracture permeability 10^{-11} m^2 (~10 Darcy)

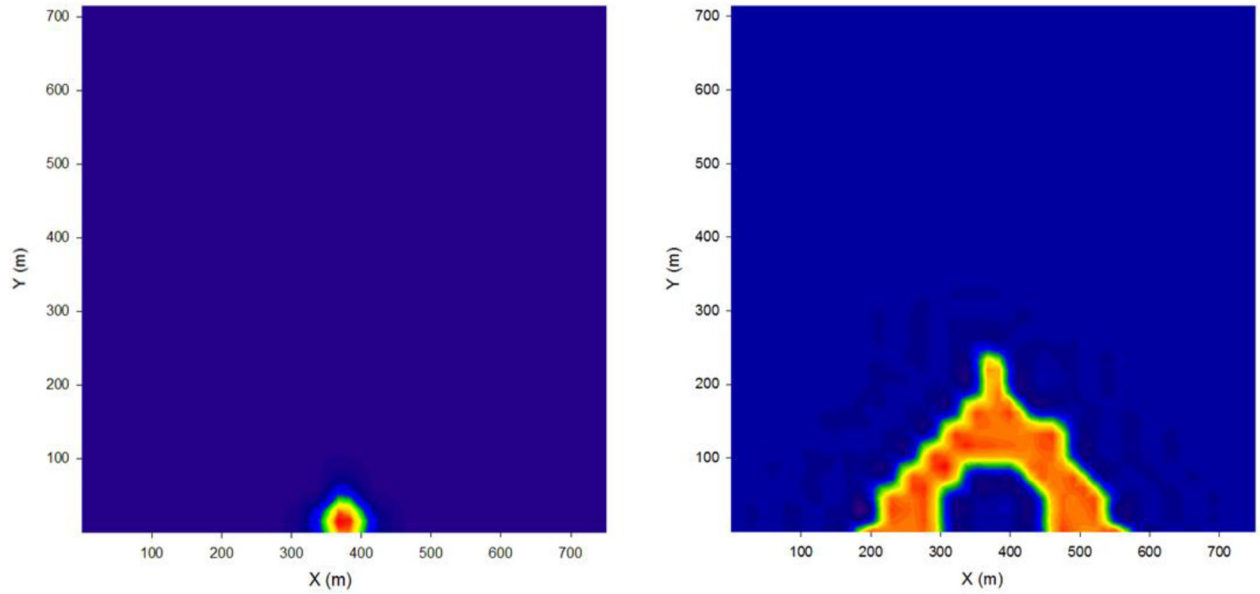

Figure 8—Distribution of high/low nonlinearity regions of Case 1. Red/orange color indicates the high nonlinearity region that is determined by the physics-based judging criteria. Blue color indicates the low nonlinearity region. The figure on the left is the distribution at 180 days of injection, while the figure on the right is that at 7 years of injection

more robust. As INB type of method requires less time spent in the linear solver within each iteration, the proposed INB-ANE method can accelerate the simulation by 10% to 30%, as demonstrated by Fig. 10 and Fig. 12.

Parallel Performance

An important property of nonlinear solvers is their parallel performance. In this subsection, we show the parallel speedup factor of INB-ANE and compare it with that of NR method. We re-run the above Case 1 with the same input parameters on a refined grid with 256*256*20 = 1,310,720 uniformly distributed grid blocks. As our simulator cannot run on a single processor, the minimum number of processors we use

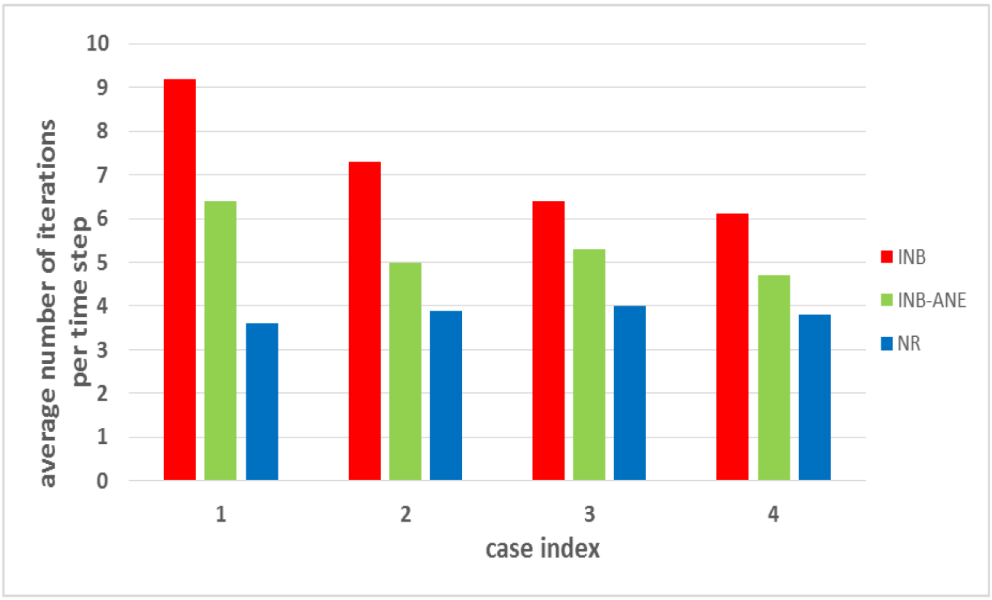

Figure 9—Comparison of the average number of iterations per time step of Case 1 to Case 4. Red columns: Inexact Newton method without preconditioning. Green columns: the proposed INB-ANE method. Blue columns: Newton-Raphson method.

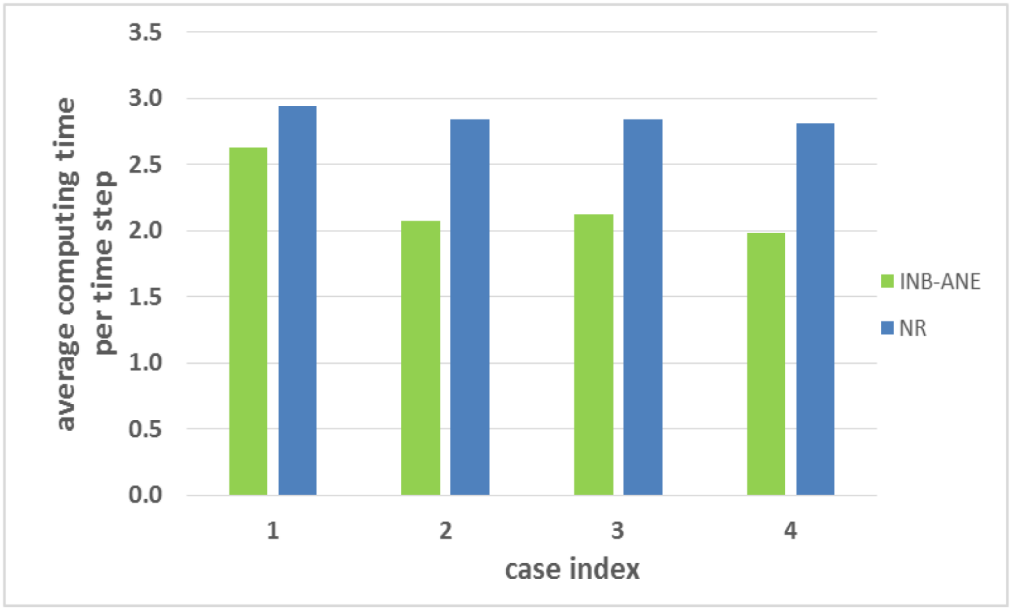

Figure 10—Comparison of the average computing time per time step of Case 1 to Case4. Green columns: the proposed INB-ANE method. Blue columns: Newton-Raphson method.

is 2. Since the parallel performance is close to linear speedup when number of processors is low enough, we use the parallel performance of the 2-processor cases as the benchmark.

As demonstrated by Table 3 and Fig. 13, INB-ANE is nonlinearly scalable, instead of linearly scalable. Compared to Newton-Raphson method, the speedup factor of INB-ANE deteriorates faster when number of processors increases. This is mainly due to the fact that the preliminary nonlinearity elimination step is not fully scalable. However, we should also notice that INB-ANE is still capable of saving around 10% of the computing time when the number of processes is 256.

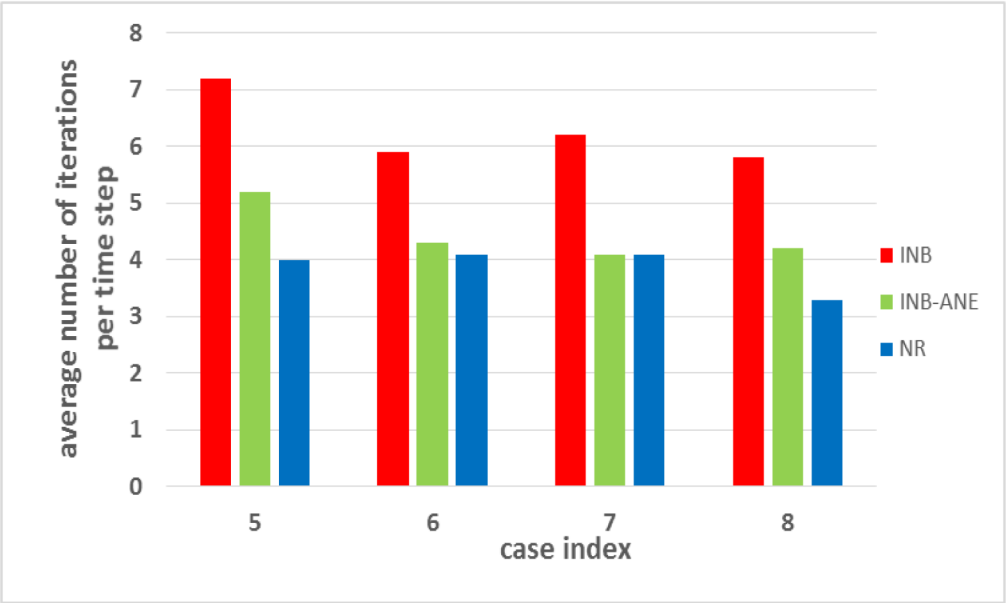

Figure 11—Average number of iterations per time step of Case 5 to Case 8. Red columns: Inexact Newton method without preconditioning. Green columns: the proposed INB-ANE method. Blue columns: Newton-Raphson method.

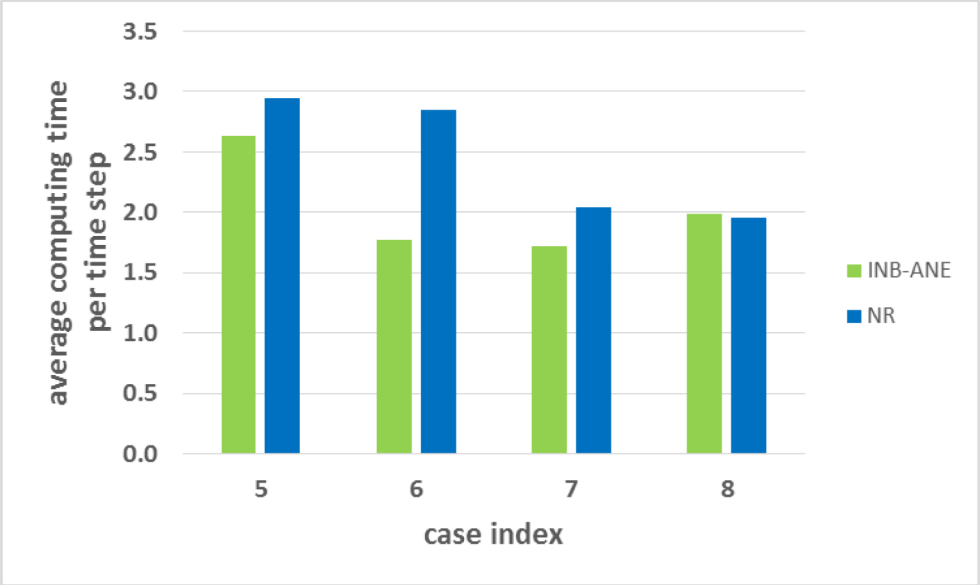

Figure 12—Comparison of the average computing time per time step of Case 5 to Case 8. Green columns: the proposed INB-ANE method. Blue columns: Newton-Raphson method.

Conclusions

We have developed a nonlinearly preconditioned Inexact Newton method, INB-ANE. The proposed method dynamically eliminates and balances the local nonlinearity/discontinuity. The method adopts a physics-based criteria to determine the high nonlinear zone within the computing domain. Using algebraic restrictors, the method can be easily implemented into the codes of existing massively parallel simulators.

We have used INB-ANE to simulate the coupled thermal-hydraulic-mechanical behaviors of fractured reservoirs with elastic-plastic effects of the fractures induced by cold water injection. It has been shown that the proposed method can improve the robustness of the Inexact Newton method, avoiding iteration

Table 3—Comparison of the parallel speedup factor of INB-ANE and NR

Number of processorses	time spent by INB-ANE (s)	speedup factor of INB-ANE	time spent by NR (s)	speedup factor of NR	Ideal (linear) speedup
2	62490.62	2	77182.2	2	2
4	32554.01	3.82	39990.78	3.86	4
8	17058.48	7.29	20581.92	7.50	8
16	9273.40	13.41	11026.03	14.01	16
32	4892.06	25.42	5629.62	27.5	32
64	2952.42	42.12	3207.90	48.12	64
128	1778.552	69.92	1946.09	79.32	128
256	1137.544	109.33	1244.87	123.32	256

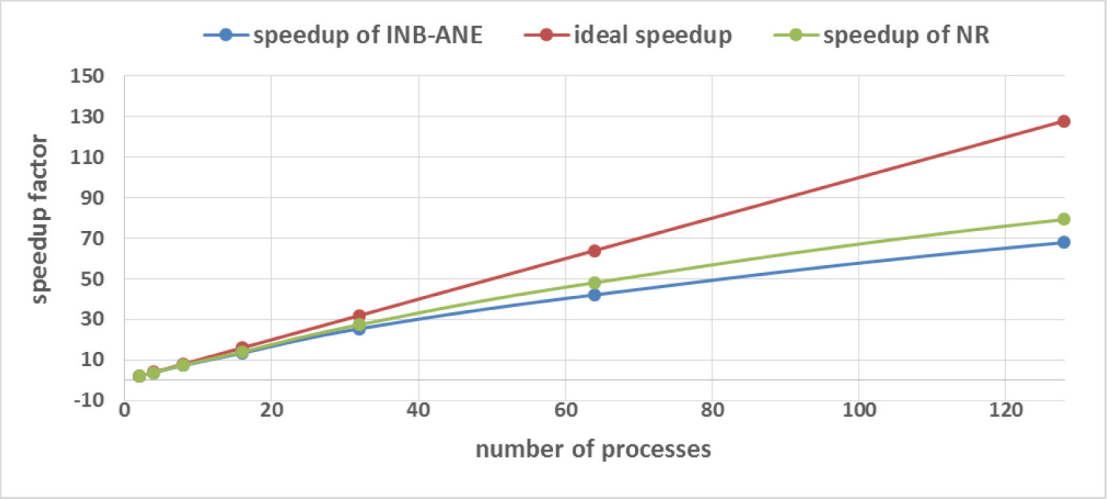

Figure 13—Comparison of the parallel speedup between INB-ANE, NR and ideal performance

failures or time step cuts. Compared to commonly used Newton-Raphson method, the proposed method can save 10% to 30% of the computing time, depending on the input parameters and the number of processors used.

The proposed INB-ANE method is a competitive nonlinear solver in simulating the tightly coupled multi-physics problems with high local nonlinearity in the practice of reservoir simulation

Acknowledgement

This work was supported by the Foundation CMG, the EMG of the Colorado School of Mines, and the National Energy Technology Laboratory of the U. S. Department of Energy.

Nomenclature

A	area of a connection
b_i	fracture aperture on the ith direction
E	Young's modulus
F	flux term
G	shear modulus
g	gravity terms
h	enthalpy
J	Jacobian matrix
K	absolute permeability

Kr	relative permeability
K_R	formation heat conductivity
K_β	liquid heat conductivity
L_i	fracture spacing on the *i*th direction
M	accumulation term
Q	generation term
p	pore pressure
Pc	capillary pressure
R	residual vector
Ri,j	resctrictor on the *i*th subdomain
S	phase saturation
T	temperature
Tm	matrix temperature
Tf	fracture temperature
Δt	length of time step
$\vec{u}$	displacement vector
u	phase specific internal energy
V	volume
v	subspace correction
X	mass component
x^k	primariy variables at the *k*th iteration step
α	Biot's coefficient
β	thermal expansion coefficient
γ	Lame's coefficient
μ	viscosity
$v_{max,hor}$	maximum horizontal stress
$v_{min,hor}$	minimum horizontal stress
ρ	density
σ'	effective stress
σ_{m}	mean stress
σ_{n}	normal effective stress
$\varnothing$	porosity

Reference

Cai, X. C., and Keyes, D. E. 2002. Nonlinearly preconditioned inexact Newton algorithms. *SIAM Journal on Scientific Computing,* **24**(1), 183–200.

Cai, X. C., Keyes, D. E., and Marcinkowski, L. 2002. Non-linear additive Schwarz preconditioners and application in computational fluid dynamics. *International journal for numerical methods in fluids,* **40**(12), 1463–1470.

Cai, X. C., and Li, X. 2011. Inexact Newton methods with restricted additive Schwarz based nonlinear elimination for problems with high local nonlinearity. *SIAM Journal on Scientific Computing,* **33**(2), 746–762.

Hwang, F. N., Lin, H. L., and Cai, X. C. 2010. Two-level nonlinear elimination based preconditioners for inexact Newton methods with application in shocked duct flow calculation. *Electronic Transactions on Numerical Analysis,* **37,** 239–251.

Hwang, F. N., Su, Y. C., and Cai, X. C. 2014. A parallel adaptive nonlinear elimination preconditioned inexact Newton method for transonic full potential equation. *Computers & Fluids*.

Karypis, G. and V. Kumar. 1995, *Metis-unstructured graph partitioning and sparse matrix ordering*

system, version 2.0.

Skogestad, J. O., Keilegavlen, E., and Nordbotten, J. M. 2013. Domain decomposition strategies for nonlinear flow problems in porous media. *Journal of Computational Physics,* **234,** 439–451.

Sun, S., Keyes, D. E., and Liu, L. 2013. Fully Implicit Two-phase Reservoir Simulation with the Additive Schwarz Preconditioned Inexact Newton Method. Paper SPE 166062 presented at the SPE Reservoir Characterization and Simulation Conference and Exhibition, 16-18 September, Abu Dhabi, UAE.

Wang, S., Xiong, Y., Winterfeld, P., Zhang, K., and Wu, Y. S. *Parallel Simulation of Thermal-Hydrological-Mechanic (THM) Processes in Geothermal Reservoirs*.

Winterfeld P. H. and Wu Y.-S. 2014 "Simulation of CO2 Sequestration in Brine Aquifers with Geomechanical Coupling," in *Computational Models for CO2 Sequestration and Compressed Air Energy Storage,* chapter 8, edited by J. Bundschuh and R. Al-Khoury, CRC Press.

Wu, Y. S. (1998). *MSFLOW: Multiphase Subsurface Flow Model of Oil, Gas and Water in Porous and Fractured Media with Water Shut-off Capability, Documentation and User's Guide*. Twange Int., Houston, Tex., Walnut Creek, Calif.